Journal of Energy Chemistry 54 (2021) 131–137

Contents lists available at ScienceDirect

Journal of Energy Chemistry

journal homepage: www.elsevier.com/locate/jechem

http://www.journals.elsevier.com/journal-of-energy-chemistry/

Heating induced aggregation in non-fullerene organic solar cells towards high performance

Baocai Du [a,b], Renyong Geng [c], Wenliang Tan [d], Yuchao Mao [a,b], Donghui Li [a,b], Xue Zhang [a,b], Dan Liu [a,b], Weihua Tang [c], Wenchao Huang [d], Tao Wang [a,b,*]

[a] School of Materials Science and Engineering, Wuhan University of Technology, Wuhan 430070, Hubei, China
[b] State Key Laboratory of Silicate Materials for Architectures, Wuhan University of Technology, Wuhan 430070, Hubei, China
[c] School of Chemical Engineering, Nanjing University of Science and Technology, Nanjing 210094, Jiangsu, China
[d] Department of Materials Science and Engineering, Monash University, Wellington Road, Clayton, VIC 3800, Australia

ARTICLE INFO

Article history:
Received 11 March 2020
Revised 19 May 2020
Accepted 21 May 2020
Available online 4 June 2020

Keywords:
Organic solar cells
Non-fullerene acceptor
Heating induced aggregation

ABSTRACT

Molecular ordering within the photoactive layer plays a crucial role in determining the device performance of organic solar cells (OSCs). However, the simultaneous molecular ordering processes of polymer donors and non-fullerene acceptors (NFAs) during solution casting usually bring confinement effect, leading to insufficient structural order of photovoltaic components. Herein, the molecular packing of m-INPOIC NFA is effectively formed through a heating induced aggregation strategy, with the aggregation of PBDB-T, which has a strong temperature dependence, is retarded by casting on a preheated substrate to reduce its interference toward m-INPOIC. A sequent thermal annealing treatment is then applied to promote the ordering of PBDB-T and achieve balanced aggregation of both donors and acceptors, resulting in the achievement of a maximum efficiency of 13.9% of PBDB-T:m-INPOIC binary OSCs. This work disentangles the interactions of donor polymer and NFA during the solution casting process and develops a rational strategy to enhance the molecular packing of NFAs to boost device performance.

1. Introduction

Bulk heterojunction (BHJ) organic solar cells (OSCs) formed upon blending polymer donors and acceptors have achieved impressive progress as promising photovoltaic technology in making lightweight, low cost and flexible energy conversion devices [1–3]. As the primary motivation, the emergence of novel photovoltaic materials especially non-fullerene acceptors (NFAs), contributes greatly to the rapid development of OSCs [4–7]. The record power conversion efficiency (PCE) of OSCs has already surpassed 18% in single-junction cells [8–11]. However, due to the relatively low crystallinity and limited exciton diffusion length in organic semiconductors, the photovoltaic conversion process in OSCs is highly depended on proper phase separation for exciton dissociation and strong intermolecular stacking for charge carrier transport [12–14].

Unlike the spherically shaped fullerene acceptors with isotropic high electron mobility [15], NFAs feature anisotropic conjugated skeletons and thus the intermolecular electron transport is strongly dependent on the closely aggregated or largely overlapped π orbits in the appropriate orientation [16–18]. The π–π stacking coherence length of the NFA has been demonstrated to be positively correlated with the device fill factor [19]. In addition, more ordered face-on stacking of NFA also contributes to the enhancement of short-circuit current density [20]. Therefore, it is critical for NFAs to form effective intermolecular stacking with the adjacent electron donors or acceptors in the blend film.

Many NFAs, e.g., ITIC and IEICO-4F, show low degree of structural ordering and are characterized by a diffusion-limited crystallization property [20–23]. In addition, many NFAs tend to be miscible with donor polymer due to their similar conjugated chemical structures [24–26]. A number of donor polymers, such as PBDB-T and PffBT4T-2OD, have been reported to show strong temperature-dependent aggregation behavior, demonstrating strong tendency to self-aggregate at low and even room temperatures [27–29]. When blending donor polymers and NFAs together, the self-aggregated donor polymers will confine the nucleation and crystallization of NFAs, resulting in the polymer aggregation dominated morphology within the blend [19,30–32]. Therefore, the

* Corresponding author at: School of Materials Science and Engineering, Wuhan University of Technology, Wuhan 430070, Hubei, China.
E-mail address: twang@whut.edu.cn (T. Wang).

https://doi.org/10.1016/j.jechem.2020.05.054

NFAs in the blends tend to form small scaled aggregates, which is unfavorable for the long range intermolecular electron transport.

Current strategies to enhance the intermolecular π–π interaction of NFAs focus on molecular tailoring and film-processing engineering [33,34], in which the synthetic modification towards the non-conjugated side chains or terminal groups of NFAs is the most effective and straight method in controlling their intermolecular assembly behavior [17,35]. For example, Hou et al. substituted the bulky hexylphenyl group of IDT-PhC6 with linear n-hexyl group, by which the reduced steric hindrance of IDT-C6 endows stronger molecular aggregation and tighter π–π stacking [17]. Beyond the molecular structure optimization, thermal annealing [36], solvent vapor annealing [37] and solvent additives [38,39], as the traditionally-used morphology modulation methods, have successfully tailored the ordering of donors and acceptors in the blends. However, the crystallinity of NFAs can be limited by the confinement effect of aggregated donor polymers to inhibit further enhancement of device performance. Therefore, it is greatly urgent to disentangle the morphology evolution processes of photovoltaic components during film casting, which will not only help optimize the active layer morphology but will also provide practical guidance for material design.

In this work, we have kinetically disentangled the confinement of aggregated donor polymer PBDB-T to the π–π stacking of non-fullerene acceptor m-INPOIC by casting the film on preheated substrates and then thermally annealing the film in sequence to encourage further order of PBDB-T. By casting the PBDB-T:m-INPOIC film on preheated substrate, the aggregation of PBDB-T is effectively retarded [28,40], hence reducing the confinement towards the diffusion of acceptor molecules to form π–π stacking. The sequent thermal annealing treatment in turn enhances the crystallization of PBDB-T and leads to the balanced aggregation in the blend with suitable phase separation, which contributes to the exciton dissociation, collection and charge carrier transport processes and therefore a maximum PCE of 13.9% of PBDB-T:m-INPOIC OSCs.

2. Experimental

2.1. Materials

m-INPOIC was synthesized in our previous work [41]. Donor polymer PBDB-T was purchased from Solarmer Materials (Beijing) Inc. ZnO precursor was prepared by dissolving 200 mg zinc acetate dehydrate ($Zn(CH_3COO)_2{\cdot}2H_2O$, 99.9%, Aldrich) and 0.056 ml of ethanolamine in 2 ml of 2-methoxyethanol. Other reagents and solvents were purchased from commercial sources and used as received.

2.2. Device fabrication

All devices in this work are based on the inverted structure of ITO/ZnO/PBDB-T:m-INPOIC/MoO_3/Ag. The pre-patterned indium tin oxide (ITO)-coated glass substrates with a sheet resistance of ≈15 Ω were sonicated in deionization water, ethanol, and isopropyl alcohol for 10 min each sequentially and keep drying at 100 °C before use. Then all substrates were explored to ultraviolet/ozone for 15 min. After that, ZnO precursor solution was spin-coated on the cleaned ITO substrates in ambient and thermal annealing at 200 °C for 30 min to form 30 nm thick ZnO film. Photovoltaic materials (D/A weight ratio is 1:1) were dissolved in chlorobenzene (with 0.5 vol% 1,8-diiodooctane (DIO)) to form 20 mg/mL solution. For the RT-cast film, active layer solution was spin-coated onto substrate at 2000 r.p.m. to obtain ≈100 nm thick film in the nitrogen-filled glove box. For the hot-cast film, the ITO substrate was preheated on a hot plate to ≈100 °C and then photovoltaic solution was spin casted at 2500 r.p.m. to obtain ≈100 nm thick film. After the filming of active layer, some devices were further thermal annealed at 100 °C for 10 min. Then the 10 nm hole transport layer MoO_3 and 100 nm Ag as the top electrode were thermally evaporated. Finally, all devices were encapsulated using epoxy inside the glove box.

2.3. Characterization

Device *J–V* characterization was conducted under AM1.5G (100 mW cm^{-2}) using a Newport 3A solar simulator (USA) in air at room temperature. The light intensity was calibrated using a standard silicon reference cell certified by the National Renewable Energy Laboratory (NREL, USA). The size of photoactive area defined by the mask with an aperture aligned with the device area was 4 mm^2. Absorption spectra were measured using a UV–visible spectrophotometer (HITACHI, Japan). Film thickness was measured using a spectroscopic ellipsometer (J. A. Woollam, USA). EQEs were measured using a Zolix (China) EQE system equipped with a standard Si diode as a reference. GIWAXS measurements were performed at Australian Synchrotron, part of ANSTO. Film simples were fabricated on Si substrates. The 12 keV X-ray beam was incident at a grazing angle of 0.2°. The morphologies of the active layers were characterized by Atomic force microscopy (AFM) (NT-MDT, Russia), and transmission electron microscopy (TEM) (JEOL, Japan).

3. Results and discussion

The chemical structures and energy levels of the donor polymer PBDB-T and NFA m-INPOIC investigated in this work are shown in Fig. 1(a) [28,41]. By leveraging the unique temperature-dependent aggregation property of PBDB-T and longer relaxation time of polymer chains [28,40], the heating-induced-aggregation (HIA) strategy could effectively manipulate the confinement effects of PBDB-T aggregates on the π–π packing of m-INPOIC molecules. As depicted in Fig. 1(b), casting the PBDB-T:m-INPOIC blend film on preheated substrate (100 °C) can retard the aggregation of PBDB-T. Hence the confinement of PBDB-T aggregates toward the ordering of m-INPOIC becomes controllable.

The UV–Vis absorption spectra are able to reveal the effects of heating induced aggregation strategy on molecular ordering processes by quantifying variations in the absorption coefficient of photovoltaic components [42,43]. According to the absorption spectra of neat PBDB-T and m-INPOIC films (shown in Fig. 2a), the peaks at around 580 and 623 nm should be attributed to the self-aggregation induced ordering of PBDB-T [28,44,45], and the peak at around 800 nm corresponds to the intermolecular packing of m-INPOIC [41]. Fig. 2(b) shows the absorption coefficient spectra of PBDB-T:m-INPOIC blend films cast under different conditions. For the film cast on preheated substrate (hot-cast), the significantly enhanced light absorption ability of m-INPOIC well indicates the heating induced stronger acceptor aggregation when comparing with the film cast at room temperature (RT-cast) [46]. The decrease in the absorption intensity of PBDB-T from hot-cast can be attributed to its retarded self-aggregation due to the enhanced temperature. Therefore, it can be concluded that the stronger aggregation of PBDB-T formed from RT-cast brings confinement effect toward the packing of acceptor molecules, with the PBDB-T aggregates restrain the diffusion of acceptor molecules to effectively pack together. After a sequent thermal annealing treatment, the simultaneously increased absorption peaks of PBDB-T and m-INPOIC are observed for the RT-cast film, implying the insufficient molecular packing of both donors and acceptors due to the mutual inter-

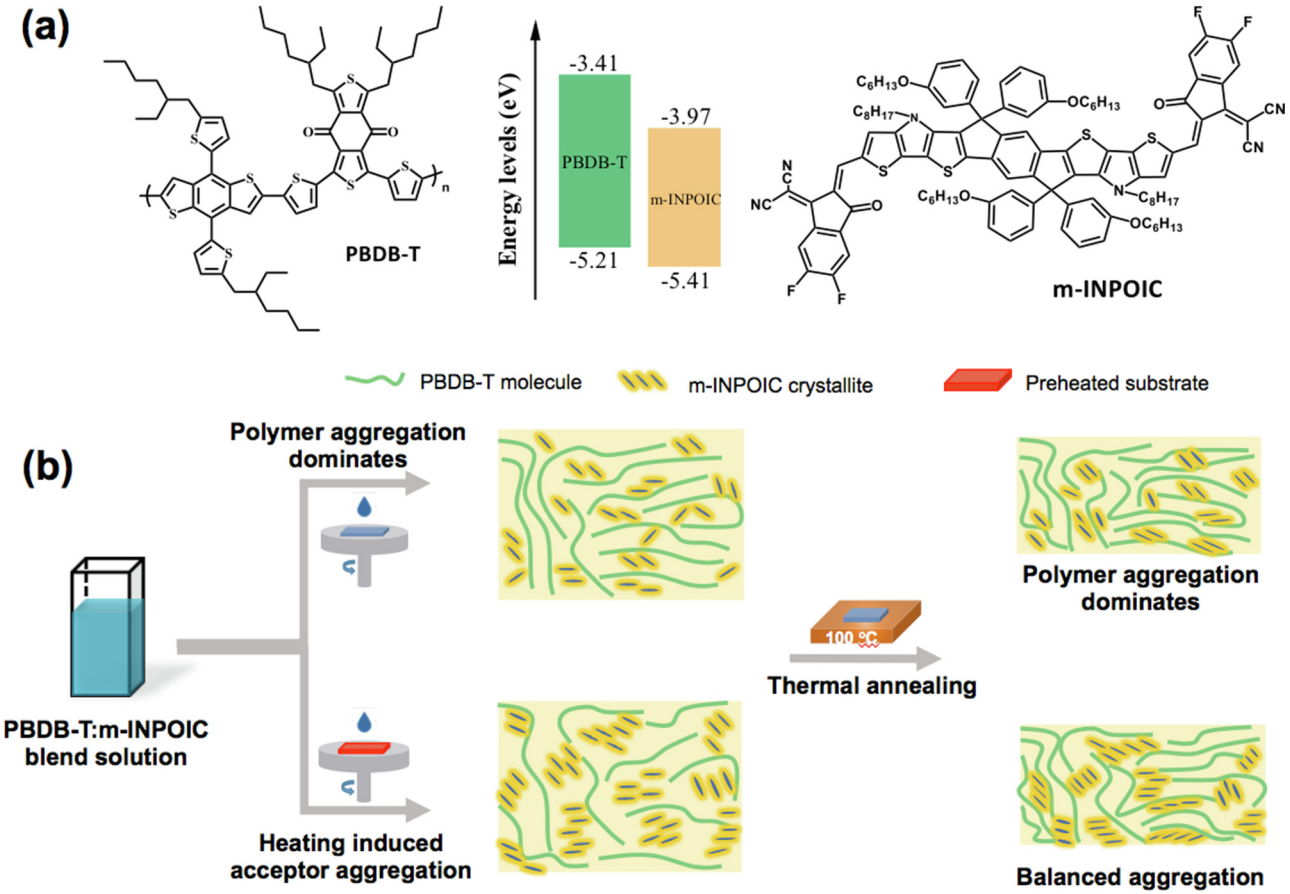

Fig. 1. (a) Chemical structures and energy levels of acceptor m-INPOIC and donor PBDB-T. (b) Schematic illustration of casting films at room temperature or on preheated substrate leads to various extend of donor/acceptor aggregation during solution casting and impacts on the further ordering of the blend during the sequent thermal annealing treatment due to the leveraging of confinement effect.

ferences during solution casting. Whilst for the thermally annealed hot-cast film, no obvious enhancement in the absorption coefficient of m-INPOIC can be observed, which confirms that the confinement effect of PBDB-T aggregates towards ordered packing of acceptor molecules during film drying has been eliminated via this HIA strategy. And the long chains of donor polymer further align orderly as signed by the significantly increased absorption coefficient of PBDB-T. The kinetically separated ordering process of PBDB-T and m-INPOIC are also beneficial towards domain purity [26] and contributes to the higher absorption intensity than the RT-cast and thermally annealed film. These different film processing approach should have significant impacts on the photovoltaic characteristics, aggregation state and phase separation of blend films, which we will discuss in the following parts.

The photovoltaic parameters of devices with an inverted structure of ITO/ZnO/PBDB-T:m-INPOIC/MoO_3/Ag are summarized in Table 1, and the device metrics from the optimization of substrate temperature are shown in Table S1. Corresponding champion device *J*–*V* curves are plotted in Fig. 2(c). The RT-cast devices show an average PCE (PCE_{avg}) of 11.2%, with a relatively low fill factor (FF) of 63.2%, short-circuit current density (J_{sc}) of 20.1 mA cm^{-2} and open-circuit voltage (V_{oc}) of 0.88 V. After further thermal annealing, the device FF and J_{sc} improve to 70.8% and 20.9 mA cm^{-2} respectively, resulting in a PCE_{avg} of 12.5% with a slightly decreased V_{oc} of 0.85 V. When the blend was cast on preheated substrate, a slightly higher PCE_{avg} of 11.4% to that of the RT-cast device was achieved, therein the FF was almost unchanged and the V_{oc} similarly decreased to 0.85 V, but the J_{sc} increased to 21.3 mA cm^{-2}. Heating induced acceptor aggregation well explains the increased J_{sc}. Additionally, the reducing of V_{oc} occurred in thermally annealed RT-cast device or hot-cast devices is similar to reported works, which could be ascribed to the changed interfacial charge transfer states [36,38,47–49]. For the thermally annealed hot-cast device, balanced aggregation in the blend contributes to the significantly increased FF of 71.4% and J_{sc} of 22.5 mA cm^{-2}, and ultimately a maximum PCE of 13.9%. Fig. 2(d) shows the external quantum efficiency (EQE) spectra of the corresponding devices, which are well associated with the J_{sc} values obtained from the *J*–*V* measurements. The changes of EQE agree well with the variations of absorption coefficient spectra and are usually attributed to the improved photon absorption and increased exciton dissociation and collection processes.

Grazing incidence wide angle X-ray scattering (GIWAXS) was conducted to investigate the confinement effects during the molecular ordering processes of neat and blend films. As shown in Fig. S1, we started the investigation from the pure films. PBDB-T displays the (1 0 0) lamellar stacking at q = 0.3 $Å^{-1}$ in both in-plane (IP) and out-of-plane (OOP) directions and the (0 1 0) π–π stacking locating at q_z = 1.72 $Å^{-1}$ in the OOP direction. The pronounced lamellar stacking peaks (2 0 0) and (3 0 0) suggest the highly ordered structure of PBDB-T, as demonstrated in previous work [50]. For the neat m-INPOIC film, distinguishable (1 0 0) lamellar packing and (0 1 0) π–π stacking diffraction peaks in both IP and OOP directions can be observed, indicating the weak structural order and uniform distributions of face-on as well as edge-on orientations. It is worth noting that the broad π–π peak of m-INPOIC

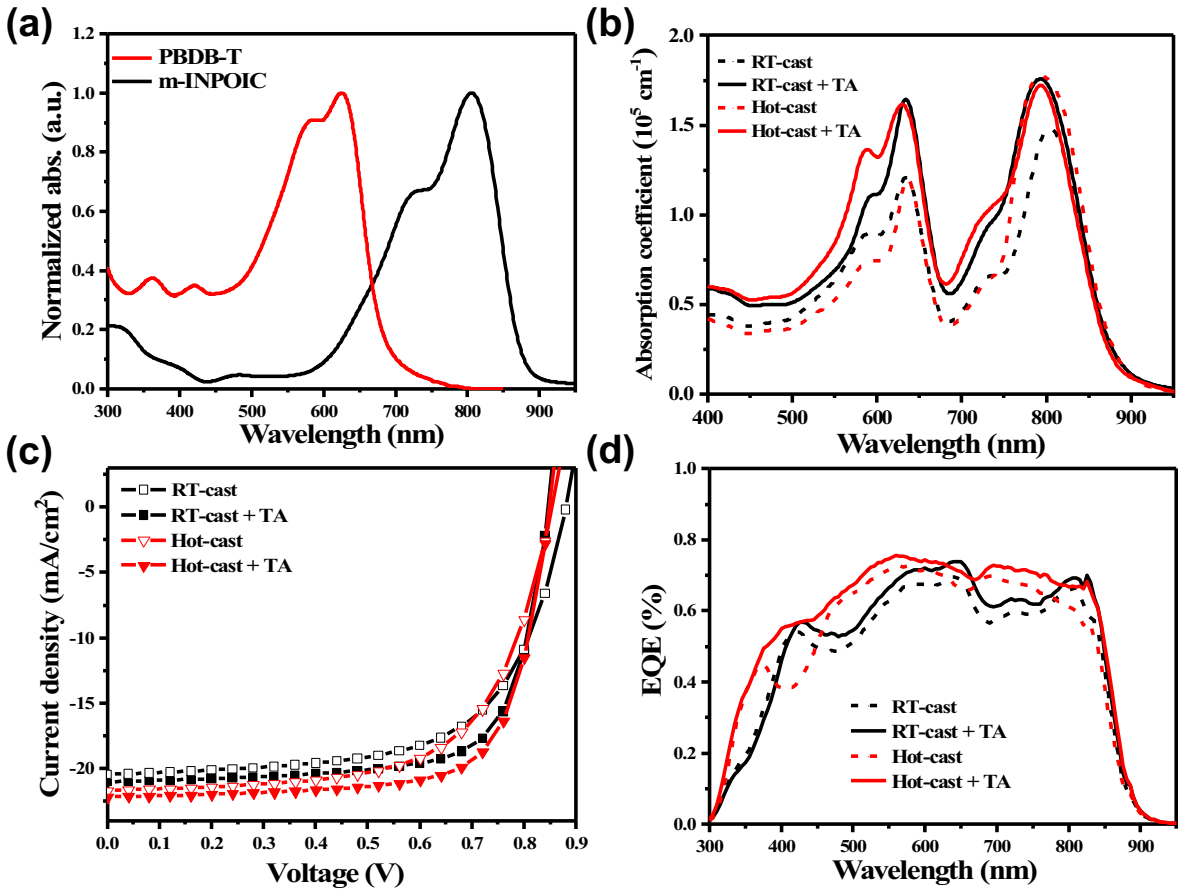

Fig. 2. (a) Normalized UV–vis absorption spectra of PBDB-T and m-INPOIC films. (b) Absorption coefficient spectra of PBDB-T:m-INPOIC films cast on normal substrate (RT-cast) or pre-heated substrate (hot-cast) and with or without the thermal annealing (TA) treatment. (c) Champion *J*–*V* curves under illumination with AM 1.5G solar simulated light (100 mW cm^{-2}) and (d) EQE spectra of the corresponding solar cells.

Table 1
Summary of photovoltaic parameters of PBDB-T:m-INPOIC devices.

PBDB-T: m-INPOIC	FF (%)	J_{sc} (mA cm^{-2})	Cal. J_{sc} (mA cm^{-2})	V_{oc} (V)	PCE_{avg} (PCE_{max}) (%)
RT-cast	63.2 ± 0.09	20.1 ± 0.23	19.1	0.88	11.2 ± 0.16(11.4)
RT-cast with TA	70.8 ± 0.45	20.9 ± 0.30	19.7	0.85	12.5 ± 0.26(12.8)
Hot-cast	64.0 ± 0.44	21.3 ± 0.90	20.7	0.85	11.4 ± 0.42(11.8)
Hot-cast with TA	71.4 ± 0.42	22.5 ± 0.13	21.4	0.85	13.6 ± 0.23(13.9)

in the OOP direction is attributed to the two overlapped diffraction peaks, located at q_z = 1.48 and 1.80 $Å^{-1}$ with the corresponding π–π stacking distances of 4.2 Å and 3.5 Å, respectively. For the A–D–A type NFAs, the different stacking distances may be resulted from the different stacking forms such as A-to-A type and A-to-D type intermolecular stacking [51]. The two-dimensional (2D) GIWAXS patterns and corresponding 1D profiles of blend films are shown in Fig. 3.

For the RT-cast blend film, the (1 0 0) lamellar stacking peak originates from the overlapping of PBDB-T and m-INPOIC signals, and the π–π stacking peak of m-INPOIC at q_z = 1.80 $Å^{-1}$ presents, suggesting the predominate face-on orientation of m-INPOIC which is conducive to the vertical charge transportation. When casting the film on a preheated substrate, the slightly decreased diffraction intensity of OOP lamellar stacking from PBDB-T, located at q_z = 0.33 and 0.96 $Å^{-1}$, proves the effectively inhibited crystallization of PBDB-T. Meanwhile, the OOP π–π stacking intensity of m-INPOIC enhances remarkably. Therefore, the HIA strategy greatly encourages the π–π stacking of m-INPOIC due to the reduced confinement effect towards the molecular packing of acceptors. After thermal annealing, the crystallinity of both RT-cast and hot-cast films get increased as shown in Fig. 3(c and d), in which the brighter scattering peaks in hot-cast and TA film are originated from the purer domains (discussed below) [52]. According to these GIWAXS results, it can be concluded that the retarded crystallization of PBDB-T during hot-cast not only encourages the face-on π–π stacking of m-INPOIC, but also promotes the crystallization of both PBDB-T and m-INPOIC without the mutual interferences during the subsequent thermal annealing process.

Atomic force microscopy (AFM) and transmission electron microscopy (TEM) were applied to probe nanoscale structural and morphological information of films prepared under different conditions. According to the AFM height images displayed in Fig. S2 and Fig. 4(a), donor polymer PBDB-T shows rope-like aggregates in the neat PBDB-T film, while neat m-INPOIC film displays a smooth and homogenous surface. When mixed together, the cotton-like PBDB-T structure dominates the surface morphology

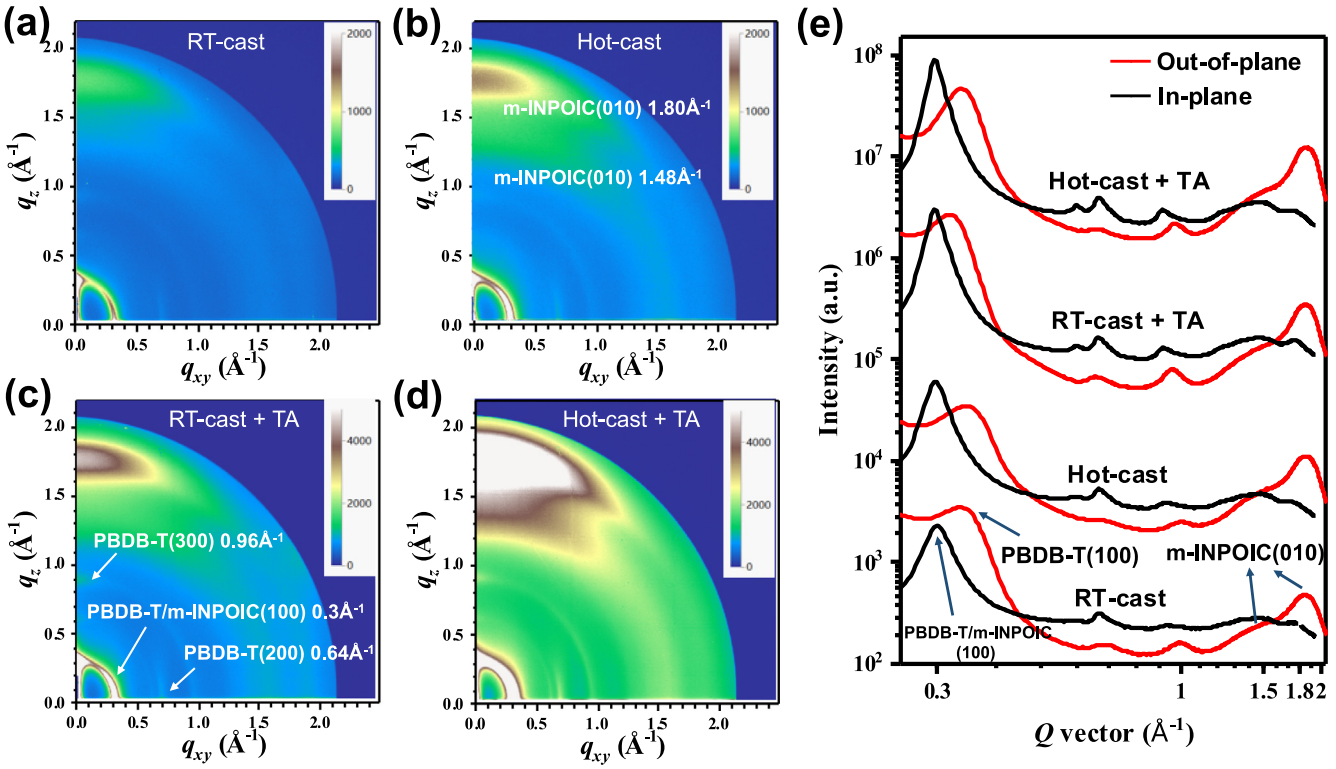

Fig. 3. Two-dimensional (2D) GIWAXS patterns of PBDB-T:m-INOPOIC blend films processed by (a) RT-cast, (b) hot-cast, (c) RT-cast with TA, (d) hot-cast with TA and (e) the corresponding 1D profiles.

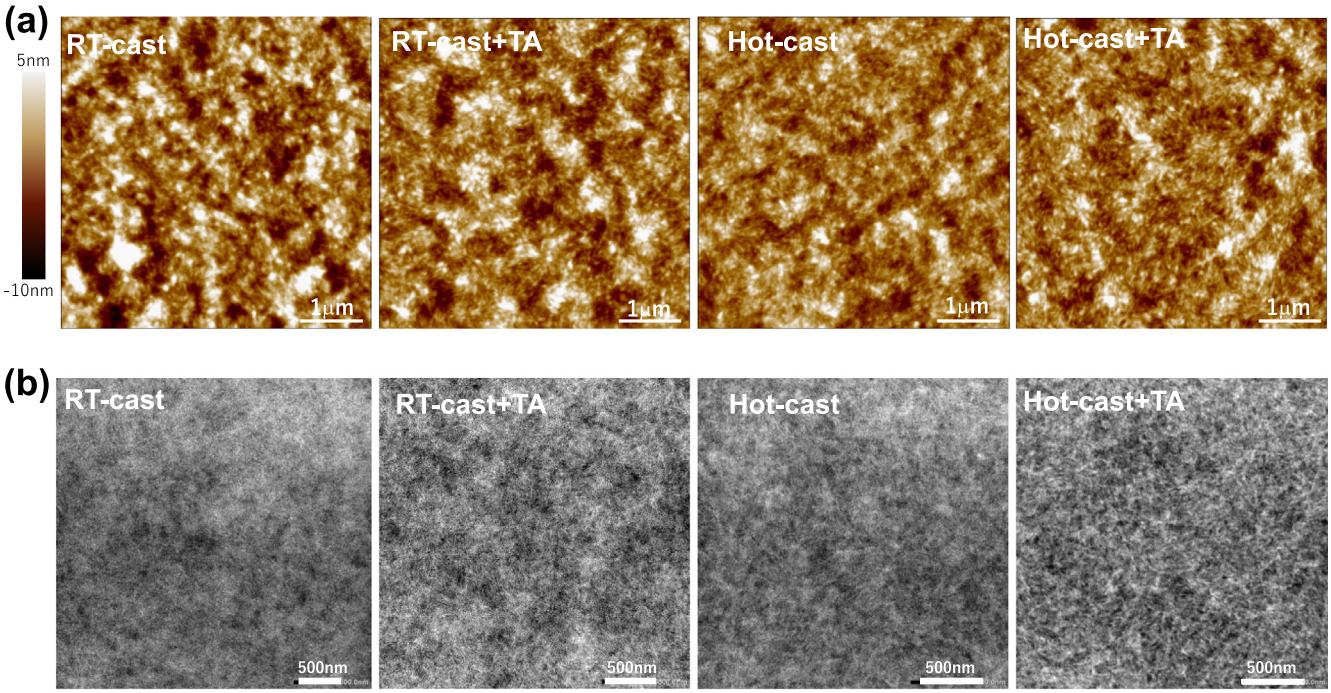

Fig. 4. (a) AFM height images and (b) TEM images of PBDB-T:m-INPOIC blend films fabricated under different conditions.

of RT-cast film. Thermal annealing intensifies the aggregation of PBDB-T and the rope-like structure becomes more obvious. By casting the film on hot substrate, the PBDB-T mainly exhibits the rope-like aggregation of chains which is conducive to charge migration and packs closer after thermal annealing [27]. The corresponding TEM images (Fig. 4b) are in agreement with AFM results. A high degree of phase separation is clearly observed in thermally annealed RT-cast film, in which the bulk PBDB-T aggregates permeate in the whole morphology. Hot-cast results in more homogeneous film morphology, and the subsequent thermal annealing further improves the continuous pathways for charge transport. The increasing J_{sc} and FF for hot-cast and TA device is in part a

Table 2
The charge carrier mobility, exciton dissociation and collection possibility of PBDB-T:m-INPOIC OSCs fabricated under different conditions.

PBDB-T:m-INPOIC	J_{sat} (mA cm^{-2})	P_{diss} (%)	P_{coll} (%)	Hole mobility (μ_h) (cm^2 V^{-1} s^{-1})	Electron mobility (μ_e) (cm^2 V^{-1} s^{-1})	μ_e/μ_h
RT-cast	21.9	94.1	78.1	1.5×10^{-4}	1.7×10^{-4}	1.1
RT-cast with TA	22.1	96.4	83.3	2.5×10^{-4}	2.9×10^{-4}	1.1
Hot-cast	22.6	98.1	82.0	1.2×10^{-4}	3.3×10^{-4}	2.9
Hot-cast with TA	24.1	98.3	87.7	3.9×10^{-4}	5.2×10^{-4}	1.4

direct result of the bicontinuous interpenetrating networks and distinguishably increased D/A interfaces.

We further investigated the impacts of crystallinity and phase separation modulated by varying the substrate temperature on the exciton dissociation, collection and charge transport properties. The charge carrier mobility (μ) of corresponding devices was evaluated via the space charge limited current (SCLC) method (shown in Fig. S3) and summarized in Table 2. For the RT-cast film, the μ_h and μ_e are 1.5×10^{-4} cm^2 V^{-1} s^{-1} and 1.7×10^{-4} cm^2 V^{-1} s^{-1}, respectively. After thermal annealing, the simultaneous enhanced crystallinity of donor and acceptor accounts for the increased μ_h of 2.5×10^{-4} cm^2 V^{-1} s^{-1} and μ_e of 2.9×10^{-4} cm^2 V^{-1} s^{-1}. When casting the film on the hot substrate, retarded crystallization of PBDB-T in the blend gave a reduced μ_h of 1.2×10^{-4} cm^2 V^{-1} s^{-1}, while the significantly increased μ_e of 3.3×10^{-4} cm^2 V^{-1} s^{-1} was attributed the heating induced acceptor aggregation and also demonstrated the crucial role of face-on π–π stacking in electron transportation. Purer phases and interpenetrating networks formed in thermally annealed hot-cast film result in enhanced electron mobility of 3.9×10^{-4} cm^2 V^{-1} s^{-1} and hole mobility of 5.2×10^{-4} cm^2 V^{-1} s^{-1} with less recombination, leading to superior device performance. According to the correlations between the photocurrent (J_{ph}) and effective voltage (V_{eff}) in various devices (shown in Fig. S3), the exciton dissociation (P_{diss}) and collection (P_{coll}) efficiencies are investigated and shown in Table 2. Here, a saturated photocurrent density (J_{sat}) will be reached at a larger V_{eff}. The J_{ph}/J_{sat} values under short-circuit and maximal power output conditions were calculated to evaluate the P_{diss} and P_{coll} in these devices. Casting the film on hot substrate creates sufficient D/A interfaces and optimal rope-like PBDB-T aggregation for exciton dissociation, which accounts for the higher J_{sc}. While the insufficient charge collection due to the low crystallinity of PBDB-T restricts the device performance with low FF. The purer phases and bicontinuous networks enable the highest P_{diss} and P_{coll} in thermally annealed hot-cast device, which contributes greatly to the achievement of the maximum device performance.

4. Conclusions

In summary, we have provided a rational heating-induced-aggregation strategy to achieve strong intermolecular π–π stacking of m-INPOIC within its photovoltaic blend with PBDB-T, and proved the significance of disentangling the confinement effect of polymer aggregation to the m-INPOIC molecular packing in enhancing device performance. During the molecular ordering processes at room temperature casting, the confinement effect from PBDB-T aggregates leads to weak structural order of m-INPOIC. Although the suboptimal morphology formed after thermal annealing facilitates charge carrier transport and exciton dissociation, inferior device PCE was achieved. While the heating-induced-aggregation strategy greatly encourages the π–π stacking of m-INPOIC but inhibits the ordering of PBDB-T by casting on a pre-heated substrate to reduce the confinement effect of PBDB-T aggregates towards the diffusion and packing of NFAs. Thermal annealing is sequentially applied to promote the molecular rearrangement of PBDB-T and achieves balanced aggregation in the blend with fine separated phases and bicontinuous interpenetrating networks to improve exciton dissociation, collection and charge carrier transport, resulting in a maximum power conversion efficiency (PCE) of 13.9%. Our results develop a fundamental understanding of the interferences for donor polymer and NFA during their molecular ordering processes and achieve enhanced intermolecular stacking of NFA by the heating-induced-aggregation strategy to benefit device performance.

Acknowledgments

This work was supported by the Natural Science Foundation of Hubei Province (Grant No. 2018CFA055) of China, and the National Natural Science Foundation of China (Grant No. 21774097). W. H. acknowledges the ACAP fellowship supported by the Australian government through the Australian Renewable Energy Agency (ARENA). GIWAXS experiments were performed at SAXS/WAX beamlines, at the Australian Synchrotron, part of ANSTO.

Appendix A. Supplementary data

Supplementary data to this article can be found online at https://doi.org/10.1016/j.jechem.2020.05.054.

References

[1] G. Li, R. Zhu, Y. Yang, Nat. Photonics 6 (2012) 153–161.
[2] L. Lu, T. Zheng, Q. Wu, A.M. Schneider, D. Zhao, L. Yu, Chem. Rev. 115 (2015) 12666–12731.
[3] T. Yan, W. Song, J. Huang, R. Peng, L. Huang, Z. Ge, Adv. Mater. 31 (2019) 1902210.
[4] G. Zhang, J. Zhao, P.C.Y. Chow, K. Jiang, J. Zhang, Z. Zhu, J. Zhang, F. Huang, H. Yan, Chem. Rev. 118 (2018) 3447–3507.
[5] H. Fu, Z. Wang, Y. Sun, Angew. Chem. Int. Ed. 58 (2019) 4442–4453.
[6] C. Yan, S. Barlow, Z. Wang, H. Yan, A.K.Y. Jen, S.R. Marder, X. Zhan, Nat. Rev. Mater. 3 (2018) 18003.
[7] J. Hou, O. Inganäs, R.H. Friend, F. Gao, Nat. Mater. 17 (2018) 119–128.
[8] Y. Cui, H. Yao, J. Zhang, T. Zhang, Y. Wang, L. Hong, K. Xian, B. Xu, S. Zhang, J. Peng, Z. Wei, F. Gao, J. Hou, Nat. Commun. 10 (2019) 2515.
[9] X. Xu, K. Feng, Z. Bi, W. Ma, G. Zhang, Q. Peng, Adv. Mater. 31 (2019) 1901872.
[10] B. Fan, D. Zhang, M. Li, W. Zhong, Z. Zeng, L. Ying, F. Huang, Y. Cao, Sci. China Chem. 62 (2019) 746–752.
[11] Z. Zhou, W. Liu, G. Zhou, M. Zhang, D. Qian, J. Zhang, S. Chen, S. Xu, C. Yang, F. Gao, H. Zhu, F. Liu, X. Zhu, Adv. Mater. (2019) 1906324.
[12] T.M. Clarke, J.R. Durrant, Chem. Rev. 110 (2010) 6736–6767.
[13] D.M. Stoltzfus, J.E. Donaghey, A. Armin, P.E. Shaw, P.L. Burn, P. Meredith, Chem. Rev. 116 (2016) 12920–12955.
[14] H.B. Naveed, K. Zhou, W. Ma, Acc. Chem. Res. 52 (2019) 2904–2915.
[15] B.C. Thompson, J.M.J. Fréchet, Angew. Chem. Int. Ed. 47 (2008) 58–77.
[16] C. Ezquerro, E. Fresta, E. Serrano, E. Lalinde, J. García-Martínez, J.R. Berenguer, R.D. Costa, Mater. Horizons. 6 (2019) 130–136.
[17] W. Su, G. Li, Q. Fan, Q. Zhu, X. Guo, J. Chen, J. Wu, W. Ma, M. Zhang, Y. Li, J. Mater. Chem. A 7 (2019) 2351–2359.
[18] V. Vohra, K. Kawashima, T. Kakara, T. Koganezawa, I. Osaka, K. Takimiya, H. Murata, Nat. Photonics 9 (2015) 403–408.
[19] H. Hu, K. Jiang, P.C.Y. Chow, L. Ye, G. Zhang, Z. Li, J.H. Carpenter, H. Ade, H. Yan, Adv. Energy Mater. 8 (2018) 1701674.
[20] X. Song, N. Gasparini, L. Ye, H. Yao, J. Hou, H. Ade, D. Baran, ACS Energy Lett. 3 (2018) 669–676.
[21] W. Zhao, D. Qian, S. Zhang, S. Li, O. Inganäs, F. Gao, J. Hou, Adv. Mater. 28 (2016) 4734–4739.
[22] L. Yu, D. Qian, S. Marina, F.A.A. Nugroho, A. Sharma, S. Hultmark, A.I. Hofmann, R. Kroon, J. Benduhn, D.-M. Smilgies, K. Vandewal, M.R. Andersson, C. Langhammer, J. Martín, F. Gao, C. Müller, ACS Appl. Mater. Interfaces. 11 (2019) 21766–21774.

[23] C. Yang, J. Zhang, N. Liang, H. Yao, Z. Wei, C. He, X. Yuan, J. Hou, J. Mater. Chem. A 7 (2019) 18889–18897.
[24] D.T. Duong, B. Walker, J. Lin, C. Kim, J. Love, B. Purushothaman, J.E. Anthony, T. Q. Nguyen, J. Polym. Sci., Part B: Polym. Phys. 50 (2012) 1405–1413.
[25] H. Cha, G. Fish, J. Luke, A. Alraddadi, H.H. Lee, W. Zhang, Y. Dong, S. Limbu, A. Wadsworth, I.P. Maria, L. Francàs, H.L. Sou, T. Du, J. Kim, M.A. McLachlan, I. McCulloch, J.R. Durrant, Adv. Energy Mater. 9 (2019) 1901254.
[26] Q. Liang, X. Jiao, Y. Yan, Z. Xie, G. Lu, J. Liu, Y. Han, Adv. Funct. Mater. 29 (2019) 1807591.
[27] Z. Zheng, H. Yao, L. Ye, Y. Xu, S. Zhang, J. Hou, Mater. Today (2019), https://doi.org/10.1016/j.mattod.2019.10.023.
[28] D. Qian, L. Ye, M. Zhang, Y. Liang, L. Li, Y. Huang, X. Guo, S. Zhang, Z. Tan, J. Hou, Macromolecules 45 (2012) 9611–9617.
[29] W. Zhao, S. Li, H. Yao, S. Zhang, Y. Zhang, B. Yang, J. Hou, J. Am. Chem. Soc. 139 (2017) 7148–7151.
[30] B. Yang, S. Zhang, Y. Chen, Y. Cui, D. Liu, H. Yao, J. Zhang, Z. Wei, J. Hou, Macromolecules 50 (2017) 1453–1462.
[31] N.D. Eastham, A.S. Dudnik, T.J. Aldrich, E.F. Manley, T.J. Fauvell, P.E. Hartnett, M.R. Wasielewski, L.X. Chen, F.S. Melkonyan, A. Facchetti, R.P.H. Chang, T.J. Marks, Chem. Mater. 29 (2017) 4432–4444.
[32] Q. Liang, J. Han, C. Song, X. Yu, D.M. Smilgies, K. Zhao, J. Liu, Y. Han, J. Mater. Chem. A 6 (2018) 15610–15620.
[33] R. Yu, H. Yao, Z. Chen, J. Xin, L. Hong, Y. Xu, Y. Zu, W. Ma, J. Hou, Adv. Mater. 31 (2019) 1900477.
[34] R.S. Gurney, D.G. Lidzey, T. Wang, Rep. Prog. Phys. 82 (2019) 036601.
[35] S. Li, L. Ye, W. Zhao, X. Liu, J. Zhu, H. Ade, J. Hou, Adv. Mater. 29 (2017) 1704051.
[36] W. Li, J. Cai, Y. Yan, F. Cai, S. Li, R.S. Gurney, D. Liu, J.D. McGettrick, T.M. Watson, Z. Li, A.J. Pearson, D.G. Lidzey, J. Hou, T. Wang, Sol. RRL. 2 (2018) 1870204.
[37] R.S. Gurney, W. Li, Y. Yan, D. Liu, A.J. Pearson, T. Wang, J. Energy Chem. 37 (2019) 148–156.
[38] L. Ye, W. Zhao, S. Li, S. Mukherjee, J.H. Carpenter, O. Awartani, X. Jiao, J. Hou, H. Ade, Adv. Energy Mater. 7 (2017) 1602000.
[39] J. Yuan, Y. Xu, G. Shi, X. Ling, L. Ying, F. Huang, T.H. Lee, H.Y. Woo, J.Y. Kim, Y. Cao, W. Ma, J. Mater. Chem. A 6 (2018) 10421–10432.
[40] Z. He, W. Shi, F. Chen, W. Liu, Y. Liang, C.C. Han, Macromolecules 47 (2014) 1741–1748.
[41] H. Feng, X. Song, Z. Zhang, R. Geng, J. Yu, L. Yang, D. Baran, W. Tang, Adv. Funct. Mater. 29 (2019) 1903269.
[42] J.L. Hernandez, N. Deb, R.M.W. Wolfe, C.K. Lo, S. Engmann, L.J. Richter, J.R. Reynolds, J. Mater. Chem. A 5 (2017) 20687–20695.
[43] Y. Mao, W. Li, M. Chen, X. Chen, R.S. Gurney, D. Liu, T. Wang, Mater. Chem. Front. 3 (2019) 1062–1070.
[44] F. Liu, Y. Gu, C. Wang, W. Zhao, D. Chen, A.L. Briseno, T.P. Russell, Adv. Mater. 24 (2012) 3947–3951.
[45] J. Lee, D.H. Sin, B. Moon, J. Shin, H.G. Kim, M. Kim, K. Cho, Energy Environ. Sci. 10 (2017) 247–257.
[46] W. Li, M. Chen, J. Cai, E.L.K. Spooner, H. Zhang, R.S. Gurney, D. Liu, Z. Xiao, D.G. Lidzey, L. Ding, T. Wang, Joule. 3 (2019) 819–833.
[47] Y. Wu, H. Yang, Y. Zou, Y. Dong, J. Yuan, C. Cui, Y. Li, Energy Environ. Sci. 12 (2019) 675–683.
[48] Q. Yue, H. Wu, Z. Zhou, M. Zhang, F. Liu, X. Zhu, Adv. Mater. 31 (2019) 1904283.
[49] S. Xie, Y. Xia, Z. Zheng, X. Zhang, J. Yuan, H. Zhou, Y. Zhang, Adv. Funct. Mater. 28 (2018) 1705659.
[50] S. Li, L. Ye, W. Zhao, S. Zhang, S. Mukherjee, H. Ade, J. Hou, Adv. Mater. 28 (2016) 9423–9429.
[51] X. Zhang, H. Wang, D. Li, M. Chen, Y. Mao, B. Du, Y. Zhuang, W. Tan, W. Huang, Y. Zhao, D. Liu, T. Wang, Macromolecules, DOI: 10.1021/acs.macromol.0c00469.
[52] L. Ye, H. Hu, M. Ghasemi, T. Wang, B.A. Collins, J.-H. Kim, K. Jiang, J.H. Carpenter, H. Li, Z. Li, T. McAfee, J. Zhao, X. Chen, J.L.Y. Lai, T. Ma, J.-L. Bredas, H. Yan, H. Ade, Nat. Mater. 17 (2018) 253–260.